Impact of phosphor granule magnitudes as well as mass proportions on the luminous hue efficiency of a coated white light-emitting diode and one green phosphor film

H. T. TUNG[1], N. D. Q. ANH[2,*], H. Y. LEE[3]
[1]*Faculty of Basic Sciences, Vinh Long University of Technology Education, Vinh Long Province, Vietnam*
[2]*Faculty of Electrical and Electronics Engineering, Ton Duc Thang University, Ho Chi Minh City, Vietnam*
[3]*Department of Electrical Engineering, National Kaohsiung University of Sciences and Technology, Kaohsiung City, Taiwan*

By using the hot pressing technique, green phosphor sheets having various silica sap/mass proportions as well as granule proportions were created. The laminated white LED (WLED) was packaged on one near-ultraviolet (n-UV) LED chip under 405 nm, and its linked hue temperature, illuminating effectiveness of radiation, light hue homogeneity, and hue coordinate were measured. The effectiveness and light hue homogeneity of the sheets as well as coated WLED device can be enhanced via elevating the mass proportion as well as decreasing the granule magnitude. These changes may also have a significant impact on the dispersion coefficient for phosphor's photonic granules as well as the effectiveness for the absorptivity-excitation-discharge activity. Using a laminate having one mass proportion reaching 6:0.75 silica sap to phosphor, the ideal value of the WLED was discovered after thorough study of various light hue parameters. The IES TM30 standard states that the R_g and chroma disparity both exhibited enhanced saturation applying to the chroma green, while the R_f achieved 92 and 101, respectively. Given that it has a light effectiveness for radioactivity reaching 270.21 lm W^{-1}, a corresponding hue heat level reaching 4423 K, and median white features, the device is ideal for lighting uses.

(Received July 27, 2023; accepted February 9, 2024)

Keywords: White LED, Lambert-Beer law, Color rendering index, Luminous efficacy

1. Introduction

Phosphor sheets (PS) are a substance that, through the activator center's transition-radiation process, is able to assimilate outer exciting photonic power then transform the power to yield one radioactivity spectrum having a particular power allocation. [1] PTF is commonly employed in a variety of industries, including solar photovoltaic generation. The transformed solar spectrum can significantly increase the efficiency of sun power use posterior to the phosphor being made into one sheet then applied onto a battery's exterior. [2, 3] The screen uniformity can be increased within a zone from one rear-illuminated screen once phosphors, like quantum points, are produced in the form of sheets via rotate daubing or sputtering. [4–6] PTFs are also applicable in the phosphor sensing sector and can be utilized for tasks like the detection of gases like O_2, CO_2, and Hg^{2+} as well as heavy metal ions like Pb^{2+} and Hg^{2+}. [7–9] PTFs can be used when it comes to solid-status illumination to enhance the illumination hue homogeneity as well as photothermic consistency for WLED devices [10, 11]. WLEDs have lately become commonly employed in the illumination and display industries. Blue-chip-based $Y_3Al_5O_{12}$:Ce (YAG:Ce) yellow phosphor excitation lacks a red spectrum and produces inferior illumination quality. A spectrum complement is therefore needed, such as the use of red phosphor. There is spectrum overlap effects between various phosphors because of the varying phosphor matrixes. [12–14] The emission spectrum will be reabsorbed by a direct hybrid coating, causing internal excitation energy consumption. Another method to produce high-quality white illumination is by using n-UV LED devices that activate triple-chroma phosphor samples, [15, 16] however it is possible to consider additional phosphor samples. One conventional mixed daubing would therefore be inappropriate when it comes to creating NUV WLEDs. The daubed PS would be intended for mitigating the spectrum's repeating absorptivity by slowing it down in accordance with the spectral properties of various phosphors. For instance, Güner [17] et al. excited red/yellow phosphors with blue LEDs. The luminous effectiveness of WLEDs can be significantly increased by putting red PS above the top of one lower yellow PS. This was mostly due to the significantly decreased likelihood for yellow illumination getting assimilated via red phosphor samples. Three main hue PTFs having emission peaks at 450, 530, as well as 620 nm were incorporated into one n-UV chip under 405 nm for creating one daubed WLED in studies conducted by Fukui [18] et al. As the radioactivity energy reached 31.2%, the color rendering index (R_a) was 95 and the illumination effectiveness reached 70 lumens/watt (lm W^{-1}).

The layered PTF structure's intermediate layer is made up of green phosphors. The efficiency of laminated WLEDs will be directly impacted by factors like phosphor transmutation proficiency (PTP) as well as illumination hue consistency since the green phosphor emission spectrum is more closely aligned with the human eye's visual efficiency curve than the blue and red ones. The absorptivity-excitation-discharge proficiency for PSes, the lumen effectiveness for radioactivity (LER), Ra, as well as illumination hue homogeneity for daubed WLEDs are all influenced by the phosphor granule magnitudes as well as mass proportions, the key parameters impacting PTF efficiency [18].

The green PS's mass proportions as well as granule magnitudes are two-dimensional variables in this investigation. The realization of the NUV WLED package is based on the layered PTF structure. Through employing power-dispersal X-ray spectroscopy visualization and assessing electronic microscopy, the phosphor allocation within PS as well as interface suitability for lattice works were examined. Excitation and emission spectra were described using the photoluminescence (PL) as well as PL excitation (PLE). The Mie dispersion theory was used to calculate the dispersion coefficients for chip discharge illumination (CDI), phosphor discharge illumination (PDI), as well as dispersing median liberal pathway (DMLP). The association between dual-dimension factors and the PCE along with reflectivity/transference was tested and calculated using a double integrating sphere (DIS). Utilizing n-UV chips under 405 nm, various laminated WLED kinds were created. The spectrum energy allocation was assessed using one nUV-observable-IR spectrometer. For identifying the dispersing allocations for CDI as well as PDI within one dual-dimension path, one illumination allocation assessor was employed. The IES TM30 standard was used to evaluate the laminated WLEDs' color indices. To determine the ideal granule magnitude as well as mass proportion in daubed WLED devices, many indices, including LER, correlated chroma temperature (CCT), as well as hue coordination, were integrated [19]. In order to create laminated PTFs and WLEDs, more research will be done after the initial study on green PTF. The objective is to investigate the characteristics of additional hue films, as well as ascertain the impact principles for various key chroma PS in daubed PS as well as WLED devices, serving as a guide to control as well as improve illumination hue efficiency.

2. Method

2.1. Phosphor preparation and creation

The used phosphors for the PTF have the following chemical formulas: Eu^{2+}-doped $(Ba,Sr)_{10}(PO_4)_6Cl_2$ (Eu-BSPC), Eu^{2+}-doped $(Ba,Sr)_2SiO_4$ (Eu-BSS), as well as $CaAlSiN_3:Eu^{2+}$ (Eu-CASN). The respective discharge spectral apexes would be under 445, 520, as well as 627 nm, with the focal granule diameter for our phosphors being 27.19, 17.86, as well as 13.18 μm. Studies reported that the blue Eu-BSPC phosphor can provide high blue luminescent property and good thermostability thanks to its apatite host structure. The green Eu-BSS has gained recognition for its high quantum efficacy, effective excitation and emission bands. Additionally, red Eu-CASN phosphor has been a favorable commercial phosphor for adding red luminescence for white LED as it owns a rigid crystal lattice exhibiting excellent performance of luminescence. These phosphors are also well-excited by NUV sources, making them suitable to applied to high-power white LED devices. Plus, combining them allows us to achieve a wide and full-spectrum band, essential to obtain the improved and efficient color rendition performance of the LED.

The used silica sap was supplied by Dow Corning Corporation and had a refraction indicator reaching 1.41 under 632.8 nm. Besides, the used $YAG:Ce^{3+}$ phosphor for the LED model exhibits an emission peak of ~570 nm. Exterior-attached apparatus lead mold dimensions for the NUV LED are 5.6 × 3 × 0.7 mm, apex wavelength reaches 405 nm. chip magnitude reaches 14 × 28 mil. Silica sap to blue phosphor mass ratio is 6: 5.5, and silica sap to red phosphor mass ratio is 6: 0.25. The creation process is displayed in Table 1.

Table 1. The processes of creating PTF and laminated WLEDs

PTF	Laminated WLEDs
- Weigh the phosphor and silica resin according to a preset mass ratio. - Stir it at a swirling rate reaching 200 rpm within twenty minutes to form a colloidal combination. - Put the mixture in a vacuum drying oven and deformed at a vacuum of 0.1 MPa for 30 minutes. - Pre-heat PTF-forming mold and spray the surface with a stripping agent. - Inject the colloidal mixture into the mold cavity to keep a temperature of 150 ^oC, time of 1.5 hours. - Cool the mold to get different serial numbers (SNs) of PTF.	- Fix the chip in the SMD lead frame by solid crystal glue; bake it in an oven at 150 ^oC for an hour. - Interconnect the electrode and lead frame electrically by a wire bonding machine. - Inject the transparent silica resin into the cavity. - Laminate and stack the PTF on the surface of the lead frame. - Bond the layers of PTF via translucent silica sap, getting rid of the air among the interfaces. - Bake it in an oven at 150 ^oC for 1.5 hours. - Fix the SMD on an aluminum substrate heat sink by applying welder mix above one welding site to achieve thermal abatement.

2.2. Characterization

The created phosphor samples' qualities were then assessed. For this inquiry, numerous tools were employed.

Table 2 provides a list of the characteristics and matching techniques.

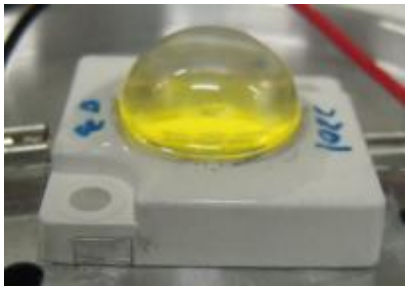

(a)

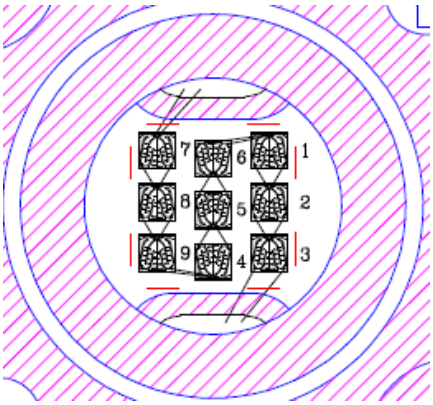

(b)

(c)

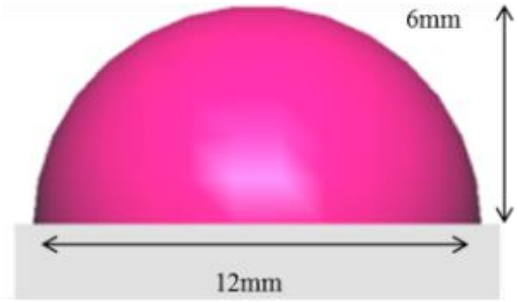

(d)

Fig. 1. WLED formation: (a) WLED apparatus, (b) Binding graph, (c) WLED design, (d) WLED simulated via LightTools

Table 2. Attributes along with assessing means

Attributes	Means
Nanoscopic form along with power spectrum for PS	Assessing electronic microscope along with tracker
Exciting along with discharge spectra	Spectrophotometer accompanied by one xenon light
R/T	Mu-lan DIS
SPD of the laminated WLED	Everfine PMS-80 NUV-observable-IR spectrometer

3. Results and discussion

3.1. Computation of the PTF luminescence

The silica resin matrix had an island-like structure with the phosphors uniformly dispersed throughout. By daubing the silica resin's –O–Si–O– malleable macrogranule frame, there are no visible channel faults at the dual-stage interface among phosphor and silica sap, showing strong interfacial continuity and compatibility. Both silica resin and phosphor have refractive indices of 1.41 and 1.8,21, correspondingly. Whole inner reflectivity (WIR) above the phosphor's exterior is less likely because of the gradient refractive index, which makes it easier for converted photons to flow from the particles' surface to the silica resin. The phosphor components are represented by the EDS visuals. The mapping diagrams for the various components are displayed. The luminescent focal point for Eu would be equally dispersed throughout the latticework. The uniform emission of light is not aided by any accumulation phenomena brought on by the phosphor's precipitating process.

All phosphors have wideband properties that make them ideal for creating wide-spectrum WLEDs. The phosphor stimulation spectrum includes the 405 nm NUV chip spectrum, which shows that it is possible to efficiently stimulate the phosphor trio through the n-UV chip. The electrical configuration of the trio is $[Xe]4f^{7}5s^{2}5p^{6}$, while their luminescence centers are all Eu^{2+}. Seven electronic granules would be placed within the $4f^{7}$ setting in the ground status of Eu^{2+}, with the ground status's spectral sign being $^{8}S_{7/2}$. The shift $4f^{7}$ between $4f^{6}5d$ for Eu^{2+}, resulting in wideband absorptivity, is where the phosphor stimulation spectra come from. Eu^{2+}'s $4f^{6}5d \rightarrow 4f^{7}$ wideband emission is represented by the discharge apexes under 445, 520, as well as 627 nm. The stimulation spans for green as well as red phosphor samples entirely enclose the spectrum of blue phosphor discharge, whereas the green counterpart would only partly encircle via the stimulation range of red phosphor. The repeating absorptivity within the formation after the combined daubing is caused by this spectral overlap effect. In order to lessen the impact of spectral reabsorption on the performance of WLEDs, the current work adopted the laminated PTF construction based on this phenomenon.

An illumination allocation assessor was employed for calculating the PDI as well as CDI dispersion distributions within one dual-dimension path for various particle and mass ratio combinations. The similarity of the PDI forward and backward distributions suggests that the isotropy principle governs the phosphor emission. An isolated CDI allocation occurs where the fore dispersing allocation span would be much greater, surpassing the rear-dispersing distribution range. According to a surge of granule amount along with the dispersion feasibility for the stimulated phosphor, the dispersion allocation span for PDI as well as CDI expands under a reduction for granule magnitude at the same mass proportion. With an increase in mass ratio, a similar equation applies, and as a result, both the granule amount as well as the dispersing amplitude rise. The stimulation photon dispersing and absorption-conversion process probability can be improved by an increase in the aforementioned dispersion amplitude.

The Mie scattering theory [20] was used to determine the DMLP for photonic transference within one PS as well as the alteration for the dispersion coefficient got PDI as well as CDI under varying mass proportions as well as granule magnitudes. The formula is as follows:

$$I_{sca} = \frac{1}{k^2 r^2}(S_{11}) I_{inc} \tag{1}$$

$$S_{11} = \frac{1}{2}\left(|S_2|^2 + |S_1|^2\right) \tag{2}$$

$$S_1 = \sum_n \frac{2n+1}{n(n+1)}(a_n \pi_n + b_n \pi_n) \tag{3}$$

$$S_2 = \sum_n \frac{2n+1}{n(n+1)}(a_n \tau_n + b_n \tau_n) \tag{4}$$

$$a_n = \frac{m\psi_n(mx)\psi_n'(x) - \psi_n(x)\psi_n'(mx)}{m\psi_n(mx)\xi_n'(x) - \xi_n(x)\psi_n'(mx)} \tag{5}$$

$$b_n = \frac{\psi_n(mx)\psi_n'(x) - m\psi_n(x)\psi_n'(mx)}{\psi_n(mx)\xi_n'(x) - m\xi_n(x)\psi_n'(mx)} \tag{6}$$

$$C_{sca} = \frac{I_{sca}}{I_{inc}} = \frac{1}{k^2 r^2}(S_{11}) = \frac{2\pi}{k^2}\sum_0^\infty (2n+1)\left(|a_n|^2 + |b_n|^2\right) \tag{7}$$

$$\mu_{sca} = NC_{sca} \tag{8}$$

The letters I_{sca} and I_{inc} stand for the strength of incident and scattered illumination, respectively. k stands for the wave numeral, r for the range between the granule focal point and the exterior position for the dispersed illumination wave, S_1, S_2 for the disperse magnitude function, a_n, b_n for the consistency symmetrical extension coefficient, π_n and τ_n for angle coefficients, x for the granule's distinctive magnitude, with m for the granule's relative refraction indicator. The Riccati-Bessel functions are denoted by $\xi_n(x)$ and $\psi_n(x)$, the dispersion cross section is denoted by C_{sca}, the dispersion coefficient is denoted by μ_{sca}, and the amount of phosphor particles is denoted by N.

For the PEL and CEL, the SMFPs and dispersion coefficient change trends and amplitudes are comparable. As the proportion of phosphors raises, the emission light dispersion coefficients linearly raise for the same particle size; the rise in the dispersion coefficient is the primary cause of this. Owing to a reduction in the distance between particles, the related SMFP displays a declining trend. For the phosphor particles to absorb stimulated photons and for the stimulation probability and conversion efficiency to rise, the SMFP must be reduced. Then, for this mass proportion, with the granule magnitude dropping, the dispersion coefficient rises whereas the DMLP falls along with it. This happens because a rise in the likelihood of photon dispersion is accompanied by a reduction in the photon propagation distance among particles.

When the mass ratio rises, the corresponding PCE does as well for particles of the same size. The particle dispersing coefficient and phosphor stimulation efficiency have increased, which is primarily responsible for this phenomenon. When the mass ratio remains constant, PCE rises as the particle size falls. CEL and PEL's respective R/T values change. When phosphor is between 80 and 95%, it means that forward propagation predominates. The value gradually rises as the mass ratio does because the composite refractive index of PTFs is rising. The refractive index difference causes the TIR likelihood to rise as the PEL reaches the film-air contact, increasing the backscattering ratio in the process.

According to the Mie scattering theory, the forward transmittance dominates light propagation, which is shown by the value of CEL, which ranges from 7 to 30%. The discharge illumination index steadily rises as the mass ratio does as well. This is brought on by the significant stimulation light absorption, particularly in the C group of small granule magnitude. When the index rises, the greatest magnitude is evident since group C has the lowest granule magnitude and the highest dispersion coefficient. Thus, the most intense amount of NUV radiation is absorbed, quickly raising the value. On the one hand, the variation in the strength of the fore as well as rear dispersed illumination would be minimal under tiny granules. Regardless, the scattered influence on the light is likewise the highest because of the enormous number of particles and dispersing coefficients. As a result, when particle size is small, the *R/T* value tends to be constant and has little bearing on the phosphor ratios.

The matching LER grows steadily while the CCT declines slowly whereas the granule magnitude as well as mass proportion rises. The dispersion factor and PCE of PTFs are both compatible with the aforementioned criterion. With an identical mass proportion, if the granule magnitude lowers, the phosphor's dispersion coefficient rises, increasing the strength of the emission. As a result,

the LER rises and the CCT falls. As the mass ratio rises for particles of the same size, the power assimilated via our phosphor samples from the stimulation illumination steadily rises as well, leading to a steady rise in emission illumination strength and a decline in CCT.

3.2. The effect of phosphor on WLED performance

The relationship between the light emission scattering factor and the dose of the PTF is shown in Fig. 2. It is possible to enhance the proportion of PTF while also enhancing the effectiveness of light transmission and wavelength conversion. As brightness rises, forward emission blue light diffusion may increase, and blue light scattering and reabsorption may decline. This is accomplished by decreasing the concentration of yellow phosphor, YGA:Ce, while increasing the concentration of PTF. As a result, the variation in the related color temperature is likewise diminished (CCT). Fig. 3 demonstrates that the concentration of YGA:Ce drops as the concentration of PTF phosphor increases, in contrast to Figs. 4 and 5, which demonstrate that CCT is concentration-invariant. With further doping, the phosphor may be able to lessen the variance in its CCT, as shown in Fig. 4. At a temperature of around 350 K, the D-CCT finally reaches its lowest value with 50% PTF, which is roughly 400 K lower than the result when 20% of PTF are used.

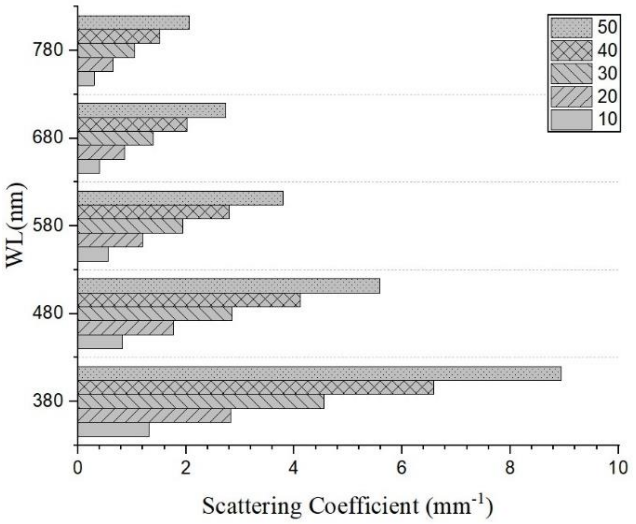

Fig. 2. Scattering coefficients with different PTF dosages

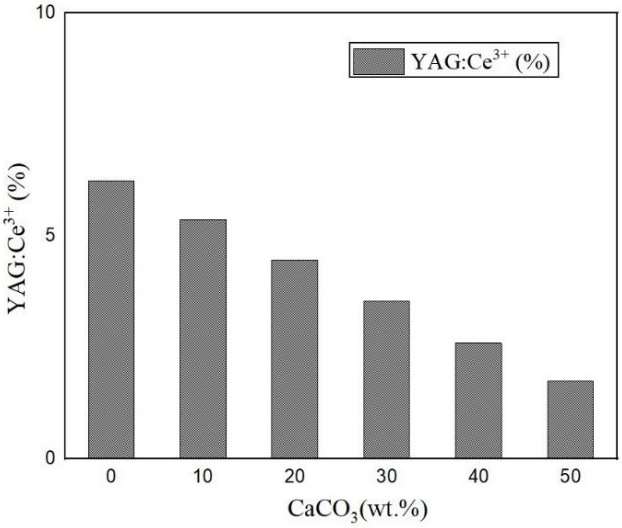

Fig. 3. YGA:Ce phosphor dosage values with different PTF dosages

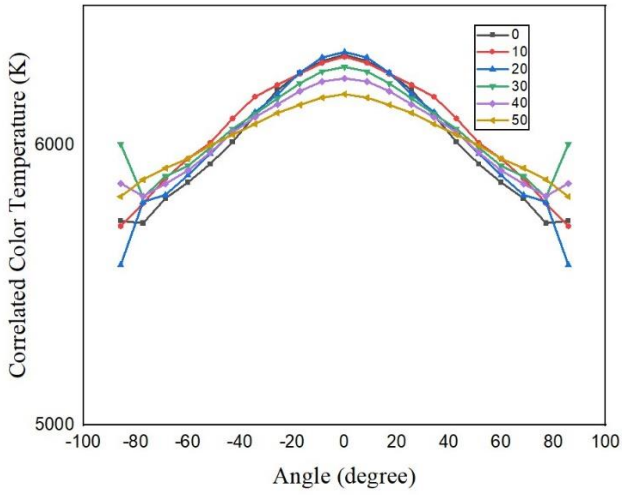

Fig. 4. CCT values with different PTF dosages

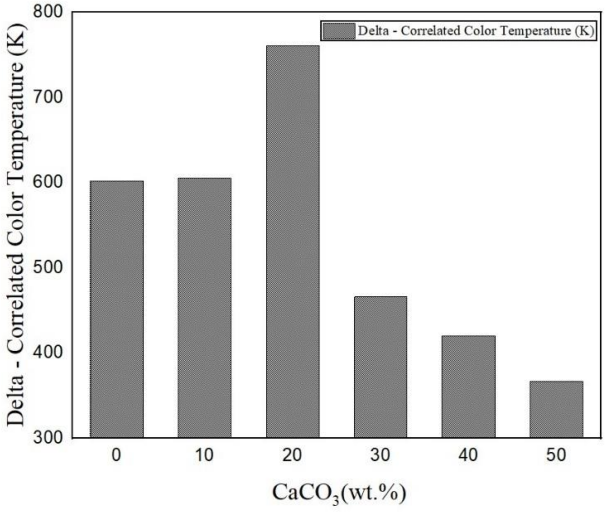

Fig. 5. Color difference values with different PTF dosages

The brightness of the white light output did not always increase when using the PTF, as seen in Fig. 6. As can be seen, the best outcomes were obtained when utilizing 50% PTF, whereas the worst results were obtained when using 0 to 10% PTF. Fig. 5 depicts D-CCT at 50% PTF, the concentration at which the decrease is greatest. As a result of increased backscattering and reabsorption, this exhibits a weaker blue emission and an uneven color distribution [21]. Higher PTF doses may promote the illumination's transmutation between blue and yellow or orange-red when our phosphor collects more backscattered blue light. The phosphor coating begins to spread once the concentration of PTF is high enough. The emission spectrum of the converted light would be restricted as a result of all the surface reflections. Another way to phrase it is that a high phosphor dose can raise CCT while lowering brightness by increasing the amount of converted light that is back-reflected. It was discovered that improving the brightness and color uniformity in the simulated WLED with a proportion of 50% PTF.

The brightness and color rendition of white LEDs are significantly affected by the amount of PTF. As the concentration of PTF reached 50%, the chroma rendition indicator (CRI) as well as chroma quality scale (CQS) were employed to assess color reproduction values, and they revealed a gradual fall. Disparate blue, green, as well as yellow-orange tendency could cause the reported declines of CRI as well as CQS [22]. The high PTF dosage causes asymmetry by increasing dispersion and tilting the color of the light emission more toward the yellow-orange region. Further study is required on this phosphor's other features, such the granule magnitude, and is subject to examination within the project herein, with the goal of manipulating CRI as well as CQS.

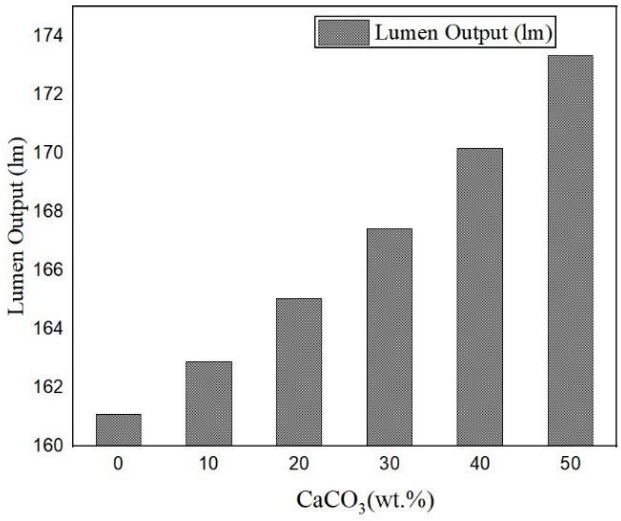

Fig. 6. Luminescence strength with different PTF dosages

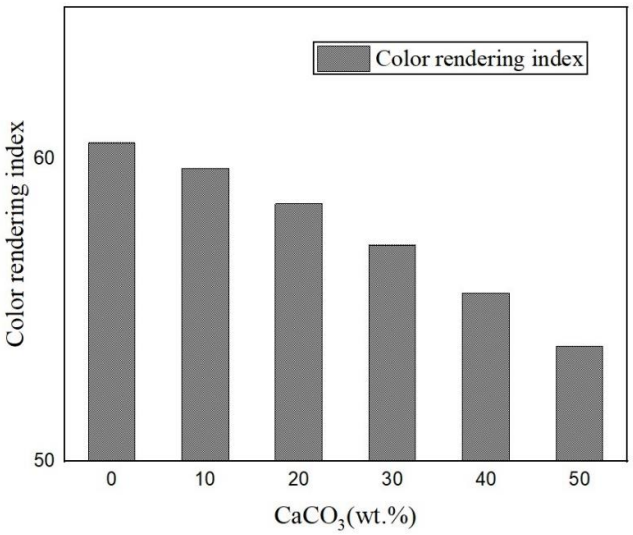

Fig. 7. CRI values of the WLED with different PTF dosages

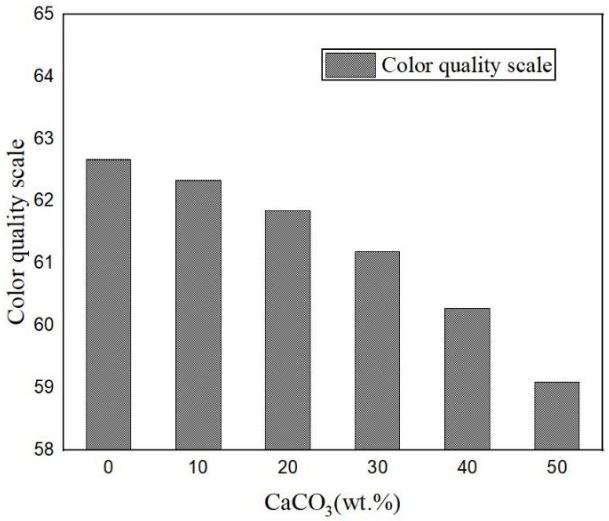

Fig. 8. CQS values with different PTF dosages

Fig. 9 exhibits the discharge bands for the PTF-based WLED. The white emission's broad spectrum highlighted the phosphor's capacity to amplify blue and orange-red light. The characteristics of the PTF can be altered to alter the patterns of light scattering and absorption and increase lighting efficacy. The peak wavelengths are in the 450 nm and ~ 600 nm ranges for blue and yellow-orange, respectively.

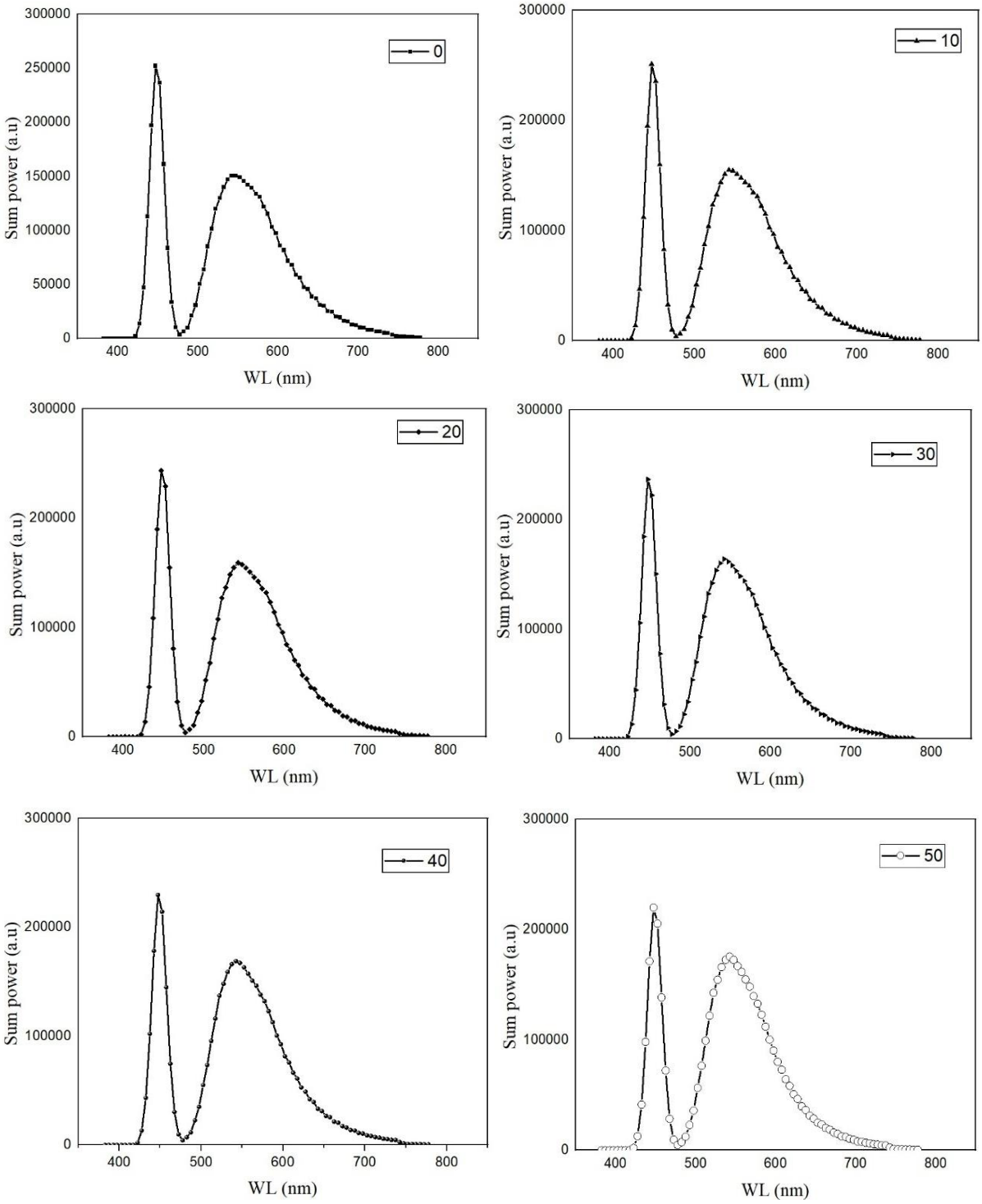

Fig. 9. Luminescence power of the WLED

4. Conclusion

By using the hot pressing technique, PSes under varied mass proportions as well as granule magnitudes were created. As the stimulation source, one chip under 405 nm was utilized, and several series of laminated WLEDs were created. Judging the dispersion activity in phosphor's granules, granule magnitudes along with mass proportions clearly alter the illumination hue attributes (like dispersion allocation, PCE, etc.) for PSes as well as daubed WLED devices. According to the enhanced dispersing probability for the excited phosphor, the dispersion allocation span for PDI as well as CDI enhanced under the reduction for granule magnitude or surge for mass proportion. Owing to the phosphor

dispersion effect, PCEs and *R/Ts* displayed comparable trends. An ideal series for dual-dimension factors (C_2 unit) was produced when many light hue indices were coupled. The LER for one daubed WLED reaches 270.21 lm W^{-1}, while the CCT reaches 4423 K under median white features. The matching mass proportion for silica sap is 6 : 0.75. In order to boost the saturation of the hue green, R_a achieved 94.2, the R_f achieved 92, while R_g hit 101. In conclusion, lighting uses are appropriate for the WLED device presented here.

References

[1] X. Huang, X. Zhao, Z. C. Yu, Y. C. Liu, A. Y. Wang, X.-J. Wang, F. Liu, Opt. Mater. Express **10**, 1163 (2020).

[2] H. S. El-Ghoroury, Y. Nakajima, M. Yeh, E. Liang, C.-L. Chuang, J. C. Chen, Opt. Express **28**, 1206 (2020).

[3] N. D. Q. Anh, P. X. Le, H. -Y. Lee, Curr. Opt. Photon. **3**, 78 (2019).

[4] Q. Xu, L. J. Meng, X. H. Wang, Appl. Opt. **58**, 7649 (2019).

[5] S. Pan, B. Yang, X. R. Xie, Z. X. Yun, Appl. Opt. **58**, 2183 (2019).

[6] Q. Zhang, R. L. Zheng, J. Y. Ding, W. Wei, Opt. Lett. **43**, 3566 (2018).

[7] T. P. White, E. Deleporte, T.-C. Sum, Opt. Express **26**, A153 (2018).

[8] A. Ullah, Y. Zhang, Z. Iqbal, Y. Zhang, D. Wang, J. Chen, P. Hu, Z. Chen, M. Huang, Biomed. Opt. Express **9**, 1006 (2018).

[9] A. Lihachev, I. Lihacova, E. V. Plorina, M. Lange, A. Derjabo, J. Spigulis, Opt. Express **9**, 1852 (2018).

[10] A. Kho, V. J. Srinivasan, Opt. Lett. **44**, 775 (2019).

[11] J.-S. Li, Y. Tang, Z.-T. Li, L.-S. Rao, X.-R. Ding, B.-H. Yu, Photon. Res. **6**, 1107 (2018).

[12] C. Zhang, B. Yang, J. Chen, D. Wang, Y. Zhang, S. Li, X. Dai, S. Zhang, M. Lu, Opt. Express **28**, 194 (2020).

[13] H. Jia, Q. J. Wu, C. Jiang, H. Wang, L. Q. Wang, J. Z. Jiang, D. X. Zhang, Appl. Opt. **58**, 704 (2019).

[14] Y. Shi, S. Ye, J. Yu, H. Liao, J. Liu, D. Wang, Opt. Express **27**, 38159 (2019).

[15] X. Yang, C. F. Chai, J. C. Chen, S. S. Zheng, C. Chen, Opt. Mater. Express **9**, 4273 (2019).

[16] S.-R. Chung, C.-B. Siao, K.-W. Wang, Opt. Mater. Express **8**, 2677 (2018).

[17] S. C. Song, X. L. Ma, M. B. Pu, X. Li, Y. H. Guo, P. Gao, X. G. Luo, Photon. Res. **6**, 492 (2018).

[18] J. H. Park, I. J. Ko, G. W. Kim, H. Lee, S. H. Jeong, J. Y. Lee, R. Lampande, J. H. Kwon, Opt. Express **27**, 25531 (2019).

[19] H. T. Tung, N. T. D. An, N. D. Q. Anh, Bulletin of Electrical Engineering and Informatics, **12**, 3388 (2023).

[20] J. Hao, H.-L. Ke, L. Jing, Q. Sun, R.-T. Sun, Appl. Opt. **58**, 1855 (2019).

[21] C. Polzer, S. Ness, M. Mohseni, T. Kellerer, M. Hilleringmann, J. Rädler, T. Hellerer, Biomed. Opt. Express **10**, 4516 (2019).

[22] H. Lee, S. Kim, J. Heo, W. J. Chung. Opt. Lett. **43**, 627 (2018).

*Corresponding author: nguyendoanquocanh@tdtu.edu.vn